Received: 22 October 2025 | Revised: 12 February 2026 | Accepted: 10 March 2026

DOI: 10.1111/joa.70141

Journal of Anatomy ANATOMICAL SOCIETY WILEY

ORIGINAL ARTICLE

Functional morphology of trabecular bone in the calcaneus of African apes

Christine M. Harper[1] | **Biren A. Patel**[2,3]

[1]Department of Anthropology, University of Washington, Seattle, WA, USA

[2]Division of Integrative Anatomical Sciences, Department of Medical Education, Keck School of Medicine, University of Southern California, Los Angeles, California, USA

[3]Human and Evolutionary Biology Section, Department of Biological Sciences, University of Southern California, Los Angeles, California, USA

Correspondence
Christine M. Harper, Department of Anthropology, University of Washington, Denny Hall, Room 146, Seattle, WA 98195, USA.
Email: cmharper@uw.edu

Funding information
National Science Foundation, Grant/Award Number: BCS-1317047 and BCS-1824630

Abstract

The relationships between whole-bone trabecular structure and mechanical loading have been well-documented in the human calcaneus. In contrast, these relationships have not been thoroughly investigated in most nonhuman primates. A recent analysis of gorillas found that calcaneal trabecular architecture varies among species generally along locomotor and ecological lines. Gorillas are the most terrestrial of the nonhuman great apes, however, which limits our comparative context to understand trabecular bone functional adaptation in both the human foot and that of closely related extant and extinct taxa. Here we analyze whole-bone calcaneal trabecular variation among a sample of both *Pan* ($n = 16$) and *Gorilla* ($n = 22$) to continue exploring the factors governing trabecular bone adaptation in the foot, as the two genera differ in both degree of arboreality and adopt variable foot postures during locomotion. Calcaneal trabecular architecture was quantified from micro-CT scans. An initial three-dimensional geometric morphometric sliding semilandmark analysis was run to position 150 volumes of interest within each bone. Trabecular thickness (Tb.Th), trabecular spacing (Tb.Sp), and bone volume fraction (BV/TV) were calculated in ImageJ and MATLAB for each VOI. Parameter distributions were summarized using principal component analysis and visualized using color maps. Non-parametric MANOVAs designed for high-dimensional data were run to test for significant differences in each parameter between genera. *Pan* and *Gorilla* significantly differ in whole-bone Tb.Th, Tb.Sp, and BV/TV ($p < 0.001$ for all analyses). Both African apes exhibit relatively higher Tb.Th and BV/TV in the anterior half of the calcaneus relative to the posterior half; however, the anteroposterior difference is exaggerated in *Gorilla*. This likely reflects a more consistent loading pattern in *Gorilla* as a consequence of their relatively more frequent use of terrestrial behaviors. *Pan* exhibits relatively higher Tb.Th and BV/TV in the calcaneal tuberosity compared to *Gorilla*, which may be indicative of a higher magnitude and frequency of forces from the triceps surae muscle complex for vertical climbing in *Pan*.

KEYWORDS
ankle, arboreal, foot, *Gorilla*, *Pan*, terrestrial

1 | INTRODUCTION

Much of comparative functional morphology research on the primate postcranial skeleton is driven by the theory of bone functional adaptation, or the broader idea that bone responds to mechanical loads (e.g., Pearson & Lieberman, 2004; Ruff et al., 2006; Ruff & Runestad, 1992; Wolff, 1892). Although much of this work has historically been carried out on cortical bone (e.g., Canington et al., 2018; Carlson, 2005; Marchi et al., 2019; Patel, 2024; Ruff et al., 2018; Sarringhaus et al., 2005; Syeda et al., 2024), studies investigating trabecular bone functional adaptation have recently become more common (e.g., Barak et al., 2011; Chirchir et al., 2017; Dunmore et al., 2019; Kivell, 2016; Ryan & Shaw, 2012; Saers et al., 2019a, 2021; Sorrentino et al., 2021; Sorrentino et al., 2022; Sylvester & Terhune, 2017). Trabecular bone is of great interest to functional morphologists because it is thought to be more metabolically active and have higher remodeling rates than cortical bone, and thus may be more responsive to the mechanical loads experienced in an individual's life (Currey, 2013; Eriksen et al., 1985; Eriksen & Glerup, 2000; Huiskes et al., 2000; Jacobs, 2000; Kivell, 2016; Sylvester & Terhune, 2017). Despite the ever-increasing number of studies investigating the relationships between trabecular architecture and locomotion, a straightforward picture of trabecular bone functional relationships has been elusive. This is likely, in part, because trabecular bone is not solely impacted by mechanical loads, but is also influenced by other factors including hormones, metabolism, and age (Boskey & Imbert, 2017; Colombo et al., 2019; Figus et al., 2022; Figus et al., 2023; Figus et al., 2025; Glatt et al., 2007; Kirchhoff et al., 2012; Lanham-New, 2008; Majumdar et al., 1997; Saers et al., 2022; Zioupos & Currey, 1998).

A growing number of studies have begun to use a whole-structure approach to investigate trabecular functional adaptation as it provides a more complete picture of the relationships between trabecular bone and mechanical loading (Bird et al., 2022; DeMars et al., 2021; Gross et al., 2014; Lukova et al., 2025; Sylvester & Terhune, 2017). Studies of whole-bone trabecular structure have been of particular interest in the foot due to its direct contact with the substrate during the stance phase of gait, and thus close contact with the substrate reaction forces (DeMars et al., 2021; Figus et al., 2022; Figus et al., 2025; Harper & Patel, 2024; Koneru & Harper, 2024; Reznikov et al., 2022; Sorrentino et al., 2021). The calcaneus makes for a particularly important model for investigating how trabecular bone in the foot varies with respect to differential loading because it plays a weight-bearing role during locomotion, has multiple articulations with other tarsal elements, and is proposed to serve as a lever for the triceps surae muscle complex (see Figure 1 for a simplified depiction of mechanical loads acting on the calcaneus). Moreover, studies have shown that variation in the external shape of the hominoid calcaneus is correlated with variation in locomotor behavior (DeSilva et al., 2019; Gebo, 1992; Harper et al., 2021; Kidd, 1999; McNutt et al., 2018; Nozaki et al., 2021; Prang, 2015, 2016). Therefore, similar relationships should be apparent in calcaneal trabecular structure.

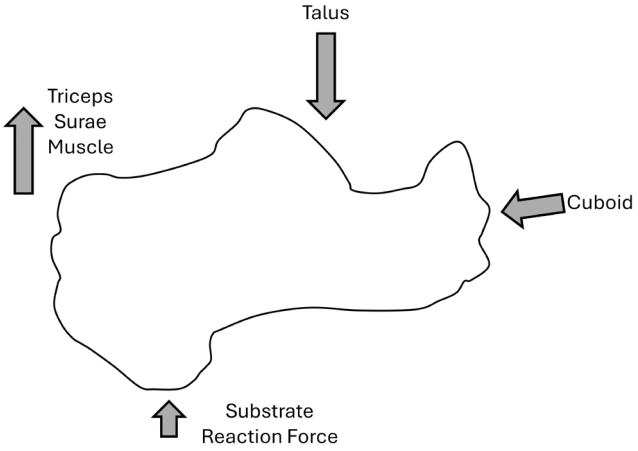

FIGURE 1 Simplified model of hypothesized mechanical forces acting on a *Pan paniscus* calcaneus (Giddings et al., 2000). This does not include ligamentous forces. Adapted from Harper & Patel (2024).

Calcaneal trabecular architecture has been relatively well-studied in modern humans (e.g., Addison & Lieberman, 2020; Athavale et al., 2010; DeMars et al., 2021; Figus et al., 2025; Gefen & Seliktar, 2004; Gierse, 1976; Koneru & Harper, 2024; Saers et al., 2019a, 2019b). Fewer studies have investigated such relationships among nonhuman primates. A recent analysis of whole-bone calcaneal trabecular structure among gorillas found that although there were some differences among *Gorilla beringei beringei*, *G. b. graueri*, and *G. g. gorilla* relative to degree of their arboreality and ecology, all gorillas demonstrate a consistent pattern of trabecular thickness (Tb.Th) and bone volume fraction (BV/TV) throughout the calcaneus (Harper & Patel, 2024). More specifically, all gorillas have relatively higher Tb.Th and BV/TV in the anterior half of the calcaneus relative to the posterior, which was hypothesized to be related to the relatively higher forces associated with body mass that are transmitted through the anterior half of the bone via the subtalar joint, compared to those forces transmitted through the posterior aspect of the bone from muscle contractions (Harper & Patel, 2024). While patterns of calcaneal trabecular bone variation have improved our understanding of foot functional morphology, these data alone are not sufficient for a full picture of calcaneal functional adaptation in hominoids, because gorillas are both the largest and most terrestrial nonhuman primates (e.g., Doran & McNeilage, 1998; Jungers & Susman, 1984; Smith & Jungers, 1997).

Due to the complexities of the relationships between trabecular bone and mechanical loading, a fine-grained stepwise approach is critical for developing a comprehensive understanding of trabecular adaptation for the nonhuman hominoid calcaneus. As such, an important next step in determining these relationships is investigating how trabecular bone varies among quadrupedal and climbing African apes, as the two extant genera vary in their frequency of arboreal behaviors and significantly differ in body mass. For example, although both *Pan* (including common chimpanzees and bonobos) and *Gorilla* engage in tree climbing, arboreal substrates constitute a larger proportion of *Pan*'s overall positional and locomotor repertoire. (Doran, 1996, 1997; Doran & Hunt, 1994; Doran & McNeilage, 1998;

Doran-Sheehy et al., 2004; Ramos, 2014; Remis, 1997, 1998a, 1998b, 1999; Robbins et al., 2025; Tocheri et al., 2011). Additionally, in both genera, females are more arboreal than males (Doran & Hunt, 1994; Remis, 1994; Doran, 1996; Doran & McNeilage, 1998; Remis, 1998a, 1998b; Ramos, 2014). Both genera also adopt terrestrial knuckle-walking as their most common form of locomotion, especially when traveling on the ground (e.g., Orr, 2005). In addition, gorillas are substantially larger in body mass than *Pan* with an average of 121.05 kg compared to an average of 43.95 kg, respectively (Jungers & Susman, 1984; Smith & Jungers, 1997). Therefore, a comparison among these two genera allows for an investigation of calcaneal trabecular bone adaptation, that is, a natural experiment.

Previous studies that have investigated trabecular bone variation in *Pan* and *Gorilla* have focused on few volumes of interest (VOIs) and thus only looked at specific regions of the calcaneus (Addison & Lieberman, 2020; Maga et al., 2006; Zeininger et al., 2016). These have found that *Gorilla* exhibits relatively higher BV/TV under the cuboid facet, Tb.Th, and Tb.Sp under the posterior talar facet, and Tb.Sp in the calcaneal tuberosity compared to *Pan* (Addison & Lieberman, 2020; Zeininger et al., 2016). While these studies have increased our understanding of calcaneal trabecular variation in *Pan* and *Gorilla*, their limited regional approach leaves potentially informative aspects of calcaneal trabecular architecture unanalyzed.

Here we investigate whole-bone patterns of Tb.Th, Tb.Sp, and BV/TV in *Pan* and *Gorilla*. We have chosen to focus on these three parameters to be consistent with previous work investigating whole-bone calcaneal trabecular structure among gorillas (Harper & Patel, 2024). We acknowledge that there is some redundancy in these three parameters, as BV/TV can be partitioned into Tb.Th and Tb.Sp. However, it is important to look at all three because different proportions of Tb.Th and Tb.Sp can lead to the same BV/TV values. Thus, investigating these three parameters in combination allows for a more nuanced picture of trabecular variation across the bone. We hypothesize that calcaneal trabecular architecture will significantly differ between the two genera and these differences will reflect their degree of arboreality as well as variable foot postures. We predict that trabecular properties will be more evenly distributed throughout the calcaneus in *Pan* than in *Gorilla* due to the likely need to adopt more variable foot positions as a consequence of greater arboreality. We additionally predict that *Gorilla* will have relatively higher Tb.Th and BV/TV than *Pan* due to the higher proposed loads associated with terrestriality and larger body size.

2 | MATERIALS AND METHODS

2.1 | Sample and image acquisition

The sample consists of representatives of *Gorilla* ($n = 22$) and *Pan* ($n = 16$) curated by the American Museum of Natural History (AMNH; New York, NY), the Harvard University's Museum of Comparative Zoology (MCZ; Cambridge, MA), the Smithsonian Institution's National Museum of Natural History (USNM; Washington, D.C.), and the Mountain Gorilla Skeletal Project (MGSP; Rwandan Government) (Table 1; see also Table S1). Although all statistical analyses are conducted at the genus level (see below), the *Gorilla* sample includes individuals representing *G. gorilla gorilla*, *G. beringei beringei*, and *G. b. graueri*, and the *Pan* sample consists of individuals representing *P. troglodytes troglodytes*, *P. t. verus*, *P. t. schweinfurthii*, and *P. paniscus*. All specimens are free from obvious skeletal pathology and are skeletally adult (i.e., all postcranial elements were fully fused). It is also important to note that the sample includes substantially more males than females for both genera (Table 1). Other than two *G. b. graueri* specimens, all specimens were wild-shot. All gorilla specimens studied here were included in a previous study by Harper and Patel (2024) of gorilla trabecular properties, including the same two captive *G. b. graueri* specimens. The study found little difference between captive and wild-shot individuals, thus supporting their inclusion in the present study (Harper & Patel, 2024). Right elements were scanned preferentially, however, when unavailable, left elements were scanned and digitally mirrored prior to analyses.

TABLE 1 Sample.

Taxon	Males	Females	Unknown
Gorilla beringei beringei	4	3	–
Gorilla beringei graueri	5	–	–
Gorilla gorilla gorilla	5	4	1
Pan paniscus	2	1	–
Pan troglodytes troglodytes	5	2	1
Pan troglodytes schweinfurthii	1	1	–
Pan troglodytes verus	2	1	–

Specimens were micro-CT scanned at voxel sizes ranging from 28 to 53 microns (Table S1). The specimens with relatively higher voxel sizes did not represent outliers in the sample. Specimens housed at the USNM and the AMNH were scanned using a GE Phoenix nanotom m system with an acceleration voltage of 100 or 120 kV and a tube current of either 80 or 190 μA at the University of Southern California's Molecular Imaging Center. The specimens housed at the MCZ were scanned using a Nikon HMXST micro-CT system with an acceleration voltage of 90 kV and a tube current of 135 μA at Harvard University's Center for Nanoscale Systems. Scan data for the MGSP specimens were provided by Drs. A. Zeininger and S. McFarlin. Scans were reconstructed as either 16-bit TIFF or DICOM images consisting of isotropic voxels. These images were segmented into binary image stacks (i.e., bone and surrounding air were segmented from each other) using the histogram-based Threshold command in ImageJ (Schneider et al., 2012; Figure 2a,b). In these binary image stacks bone is represented by white voxels and air is represented by black voxels (Figure 2b). Surface models were generated from micro-CT data in Avizo Lite 9.0.1 (FEI Visualization Sciences Group, 2015) and were cleaned (i.e., non-bone elements removed, and small holes filled) in Geomagic Wrap (3D Systems, 2015). Using digital calipers, femoral head superoinferior breadth was measured (when available) for use in body mass estimation (discussed below).

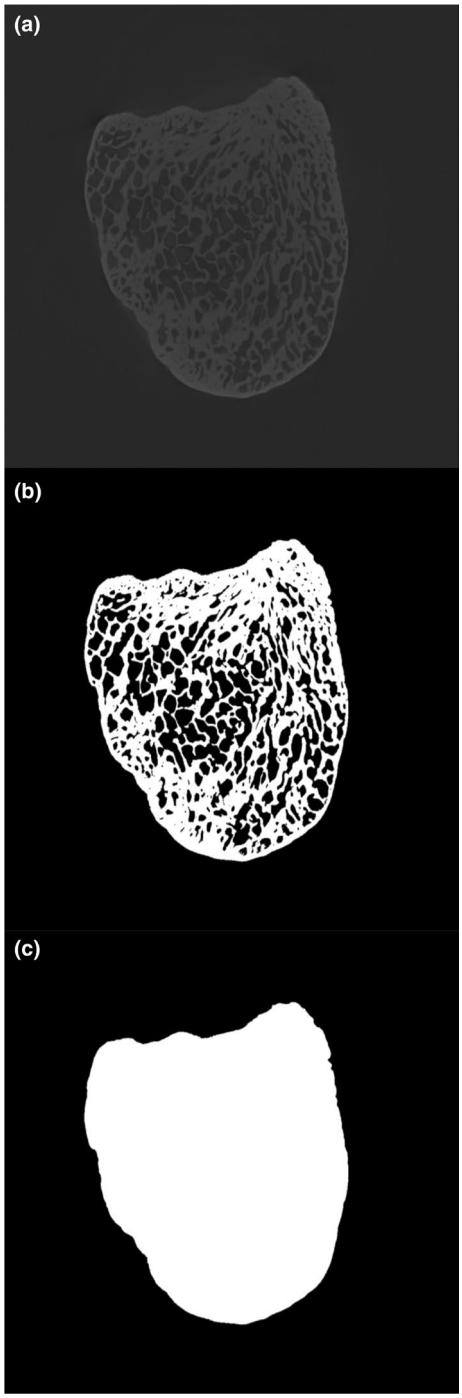

FIGURE 2 Micro-CT data processing for a *Pan troglodytes* calcaneus. The images are as follows: (a) the original Tiff image, (b) a binary segmented image (bone represented in white, air in black), and (c) a bone mask.

2.2 | Sliding Semilandmark analysis and volume of interest positioning

Volumes of interest (VOIs) were consistently positioned in the same relative location within each calcaneus based on the outputs of a three-dimensional geometric morphometric (3D GM) sliding semilandmark analysis (Gunz et al., 2005; Sylvester & Terhune, 2017). For the 3D GM analysis, calcaneal external shape was represented by 1007 sliding semilandmarks following Harper et al., 2021 (Figure S1). Curve semilandmarks (91 total) were hand-placed on the margins of the anterior/middle talar, posterior talar, and cuboid articular facets of each specimen. The 916 surface semilandmarks were manually placed on a single template specimen and warped to all other specimens using the thin plate spline (TPS) interpolation function established using the 91 curve semilandmarks and 15 (unanalyzed) orientation landmarks. The orientation landmarks were solely used to position the surface semilandmarks into a starting position for sliding (see additional details of this methodology in Harper, 2023). These warped semilandmarks were then projected onto the calcaneal surface.

Curve semilandmarks were allowed to slide along tangent vectors and surface semilandmarks along tangent planes to minimize the bending energy of the TPS interpolation function relative to a reference specimen in MATLAB v. 2022b (Mathworks, Inc., Natick, MA). As semilandmarks can sometimes slide off the bone during this process, they were then projected back onto the bony surface (Gunz et al., 2005). These landmark configurations then underwent a Generalized Procrustes Analysis (GPA) to remove the effects of size, location, and orientation (Gower, 1975; Rohlf & Slice, 1990). The average of the Procrustes coordinates was calculated and used as the reference specimen in the next round of sliding. This process of sliding, projecting, and GPA was carried out for three rounds, at which point the average of the Procrustes coordinates (rounded to four decimal points) ceased to change.

One hundred forty-six spherical VOIs were positioned using a 3D version of Lloyd's algorithm, also known as a Voronoi iteration, (Lloyd, 1982) into a single template specimen in MATLAB 2022b (Mathworks, Inc.; Figure 3). An additional 48 VOIs were manually positioned in the sustentaculum tali of the template because it was not possible to place VOIs in this region of the calcaneus using an automated placement method due to its narrow morphology (Harper & Patel, 2024). For our initial VOI placement, we began with the same number of VOIs as used in Harper and Patel (2024). An important step in the process is to visually inspect all VOIs to ensure that none include cortical bone. Any VOIs that included cortical bone were excluded from the analysis. There were six VOIs that were originally included in the gorilla-only analysis (Harper & Patel, 2024) that had to be removed for this analysis, which we postulate is related to differences in relative cortical bone thickness between the taxa. These VOIs were then warped into all other specimens using the TPS interpolation function based on the 3D GM analysis final landmark configurations following Sylvester and Terhune (2017). This approach ensures that the VOIs are in geometrically homologous locations within each bone and thus the trabecular variation can be statistically analyzed. To ensure that the VOIs represented homologous bone volumes across specimens that vary in size, all VOIs were scaled as a percentage of total bone volume (Fajardo et al., 2007; Kivell et al., 2011; Lazenby et al., 2011). Total bone volume was calculated for each calcaneus in Avizo Lite 9.0.1 (FEI Visualization Sciences Group, 2015). Those VOIs positioned in the

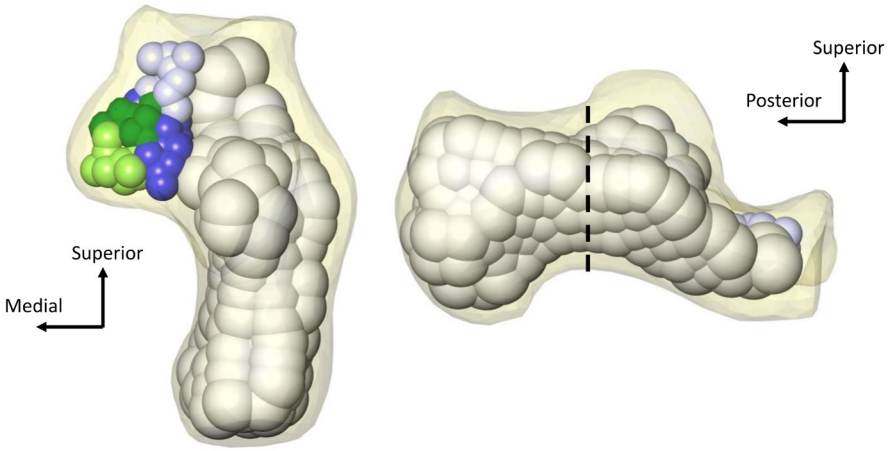

FIGURE 3 The average *Pan troglodytes* calcaneus with volumes of interest (VOIs; represented by the white spheres) positioned in the bone based on a three-dimensional geometric morphometric sliding semilandmark analysis from a superior (left) and lateral (right) view. One hundred forty-six VOIs were placed in the calcaneus using a 3D version of Lloyd's algorithm and scaled to 1.5% total bone volume. An additional 48 VOIs were hand-placed in the sustentaculum tali and scaled to 0.13% total bone volume. To ensure these smaller VOIs did not play an outsized role in the analysis, they were combined to create four larger VOIs (color coded by larger VOI assignment). The dashed line indicates the cutoff between the anterior and posterior halves of the bone for the ratio analyses.

sustentaculum tali were scaled to 0.13% total bone volume (average radius 2.21 mm), while all other VOIs were scaled to 1.5% total volume (average radius 4.97 mm) following Harper and Patel (2024). The VOIs in the sustentaculum tali were scaled to a smaller bone percentage to ensure that they did not include any cortical bone; when using 1.5% total bone volume, the sustentaculum tali VOIs projected outside of the bone. To prevent the sustentaculum tali from playing a disproportionate role in the analysis, these sustentacular VOIs were combined to create "larger" VOIs totaling approximately 1.5% total bone volume (Figure 3).

2.3 | Trabecular bone parameter calculation

For each VOI, trabecular thickness (Tb.Th), trabecular spacing (Tb.Sp), and bone volume fraction (BV/TV) were calculated following Sylvester and Terhune (2017). The Thickness function in the BoneJ plugin for ImageJ was used to calculate Tb.Th and Tb.Sp (Doube et al., 2010; Schneider et al., 2012; Sylvester & Terhune, 2017). For Tb.Th, this function was applied to the segmented image stack (Sylvester & Terhune, 2017). For Tb.Sp, however, the Thickness function was applied to an image stack in which trabecular spaces are represented by white voxels and both the bone and surrounding air are represented by black voxels (Sylvester & Terhune, 2017). A new image stack that mirrors the original is output from the Thickness function in which the values of the white voxels from the original binary image stacks are replaced with those representing the local thickness levels of the bone (or space for Tb.Sp; Doube et al., 2010). The values within each VOI were then extracted from both the thickness and spacing stacks and the average thickness and spacing values for the respective VOIs were calculated. To calculate BV/TV an image stack was first generated in which the entire internal structure of the calcaneus is represented by white voxels (i.e., a bone mask; Figure 2c) in MATLAB 2022b (Mathworks Inc., Sylvester & Terhune, 2017). Bone volume fraction was then calculated as the ratio of white voxels in each VOI of the segmented image stack to the number of white voxels in the same VOI of the bone mask in MATLAB 2022b (Mathworks, Inc.; Sylvester & Terhune, 2017). We chose not to measure degree of anisotropy, another widely reported trabecular parameter, due to some of the complexities of interpreting this measure for the whole-calcaneus without information on trabecular orientation.

2.4 | Body mass estimation

Body mass was estimated using the African ape regression equation from Burgess et al. (2018) based on the relationship between femoral head superoinferior breadth to known body masses from wild-caught primates. Three specimens were excluded from analyses utilizing estimated body mass (EBM) because femoral head SI breadth was not available (Table S1).

2.5 | Statistical analyses

For all analyses (unless otherwise stated), the alpha value was set to 0.05. In addition to analyzing raw parameter values, parameter value z-scores for each VOI were analyzed to investigate patterns of parameter distribution throughout the calcaneus without the influence of magnitude (Sylvester & Terhune, 2017). Whole-bone raw parameter and z-score variation was summarized using (separate) principal component analyses (PCA) in MATLAB 2022b (Mathworks, Inc.). A non-parametric version of a multivariate analysis of variance (MANOVA) designed for high-dimensional data (Collyer et al., 2015) was run to

test for significant differences between *Pan* and *Gorilla* in both raw parameter values and z-scores for all trabecular properties. The non-parametric MANOVAs were run in the R statistical environment using the geomorph package (Adams & Otárola-Castillo, 2013; R Core Team, 2021; Collyer et al., 2015). Both raw value and z-score parameter distributions were visualized using color maps of *Pan* and *Gorilla* averages in Avizo Lite 9.0.1. (FEI Visualization Sciences Group, 2015). Following Harper & Patel, 2024, ratios of trabecular parameters of the VOIs in the anterior half of the bone relative to those in the posterior half (Figure 3) of the bone were calculated to investigate regional variation among the genera. The most posterior point of the posterior talar facet was defined as the anterior–posterior dividing line and all VOIs that were completely (or primarily) located anterior to the line were considered anterior, while those posterior to the line were considered posterior (Figure 3). Ratios were analyzed using Wilcoxon rank sum tests run in MATLAB 2022b and visualized using boxplots.

The role of body size in trabecular variation was evaluated using reduced major axis (RMA) regressions run in the R statistical environment using the lmodel2 package (R Core Team, 2021). The average whole-bone raw parameter value for each specimen was regressed against EBM in natural log-natural log space. Reduced major axis regressions were used because they assume error in both the x and y terms and that the variance within these two terms is proportional to that error (Sokal & Rohlf, 1998; Swartz & Biewener, 1992). For BV/TV, a slope of 0 was considered isometric, while a slope of 0.33 was considered isometric for Tb.Th and Tb.Sp. The relationships between the trabecular parameter of interest and EBM were considered non-isometric if the 95% confidence interval did not include isometry. ANCOVAs were performed using the smatr package in the R statistical environment to test for significant differences in slope between the genera (Warton et al., 2012).

3 | RESULTS

Summary statistics for all trabecular parameters are presented in Table 2.

3.1 | Tb.Th

Pan and *Gorilla* significantly differ in whole-bone Tb.Th raw parameter values ($p=0.001$). When the raw parameter values are examined, the two genera exhibit some separation across PCs 1–3 (77.93% of the variance); however, there is more variation in Tb.Th in *Gorilla*

TABLE 2 Summary statistics of whole-bone raw trabecular parameters.

Genus	Tb.Th	Tb.Sp	BV/TV
Gorilla	0.420 (0.157)	1.066 (0.256)	0.276 (0.084)
Pan	0.320 (0.094)	0.890 (0.394)	0.316 (0.095)

Note: Means and standard deviations (in parentheses).

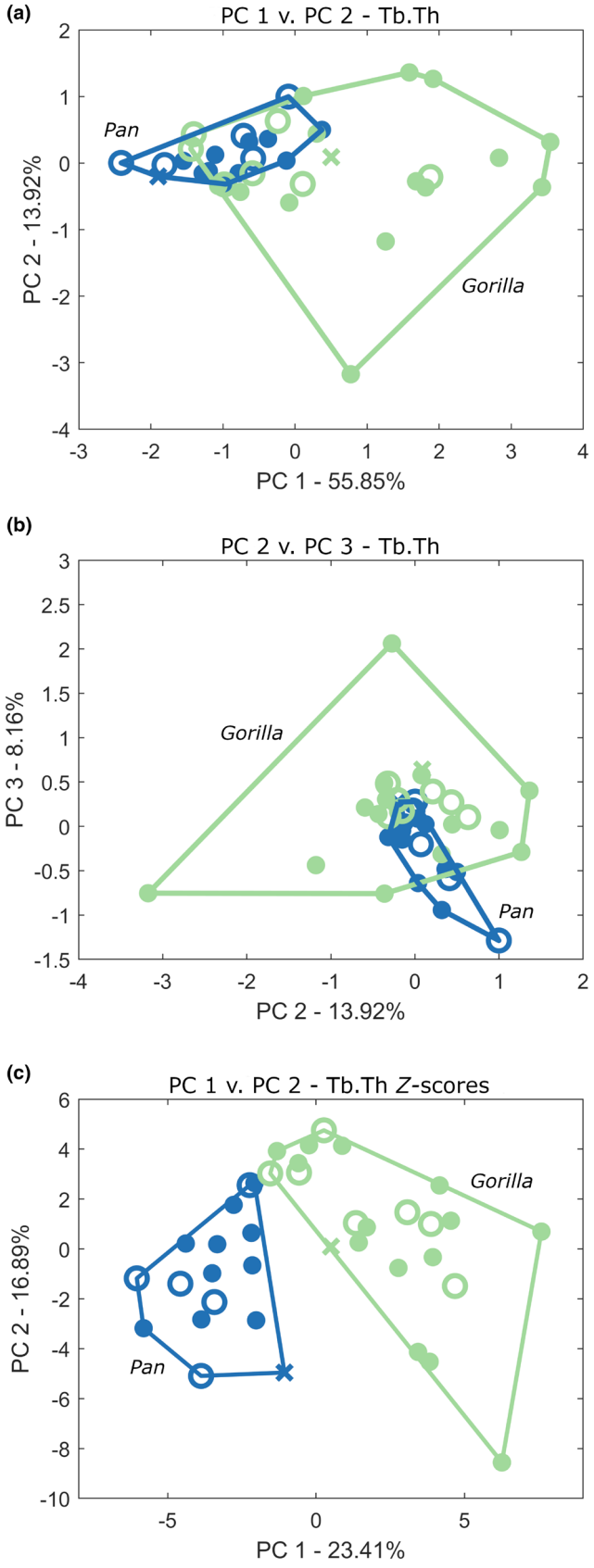

FIGURE 4 PC plots of (a-b) whole-bone raw Tb.Th and (c) Tb.Th z-scores. *Gorilla* is in green, and *Pan* is in blue. Males are represented by closed circles, females open circles, and specimens of unknown sex are represented by crosses.

(Figure 4a,b). For both genera, trabeculae are relatively thicker in the anterior half of the bone; however, this anterior to posterior difference in raw parameter values is significantly greater in *Gorilla* ($p = 0.008$; Figures 5a and 6a). There were no significant differences in RMA slope between *Pan* and *Gorilla* when Tb.Th is regressed against EBM. In the pooled sample, Tb.Th is significantly correlated with EBM ($p < 0.001$) and scales with slight positive allometry; however, the 95% confidence interval does include isometry (Figure 7a; Table 3).

Pan and *Gorilla* also significantly differ in whole-bone Tb.Th z-score values based on the non-parametric MANOVA ($p = 0.003$) and there is clear separation between *Pan* and *Gorilla* along PCs 1–2 (40.3% of the variance; Figure 4c). Compared to *Gorilla*, *Pan* exhibits concentrations of relatively thick trabeculae anteriorly and in the calcaneal tuberosity (Figure 6b). *Gorilla* also exhibits thicker trabeculae along the plantar surface (Figure 6b).

3.2 | Tb.Sp

Pan and *Gorilla* significantly differ in whole-bone Tb.Sp raw parameter values ($p = 0.001$). When raw parameter values are examined, the two genera separate from each other along PCs 1–2 (79.24% of the variance; Figure 8a; PCs 2–3 are illustrated in Figure S2a). The *Pan* calcaneus is characterized by less spacing overall than the *Gorilla* calcaneus; however, there is significantly more spacing in the anterior half of the bone relative to the posterior in *Pan* (Figures 6b and 9a). There were no significant differences in RMA slope between *Pan* and *Gorilla* when regressed against EBM. In the pooled sample, Tb.Sp is significantly related to EBM ($p = 0.006$) and scales with isometry (Figure 7b; Table 3).

Pan and *Gorilla* also significantly differ in whole-bone Tb.Sp z-scores ($p = 0.003$), indicating a different distribution of spacing throughout the calcaneus. PCA results for Tb.Sp z-scores are presented in Figure S2b. Compared to *Gorilla*, *Pan* exhibits a relatively larger concentration of spacing in the anterior calcaneus, particularly underlying the posterior talar facet (Figure 9b).

3.3 | BV/TV

Pan and *Gorilla* significantly differ in whole-bone BV/TV raw parameter values ($p < 0.001$). The two genera separate from each other along PCs 1–2 (68% of the variance; PCs 2–3 are illustrated in Figure S3a) when raw parameter values are examined (Figure 8b). *Gorilla* exhibits relatively higher BV/TV in the anterior calcaneus relative to the posterior than *Pan* (Figures 6c and 10a). This is likely driven by the relatively higher BV/TV in the calcaneal tuberosity in *Pan* (Figure 10a). There was no significant relationship between BV/TV and EBM (Figure 7c).

When z-scores are examined, there are significant ($p < 0.001$) differences between *Pan* and *Gorilla* in whole-bone BV/TV (see

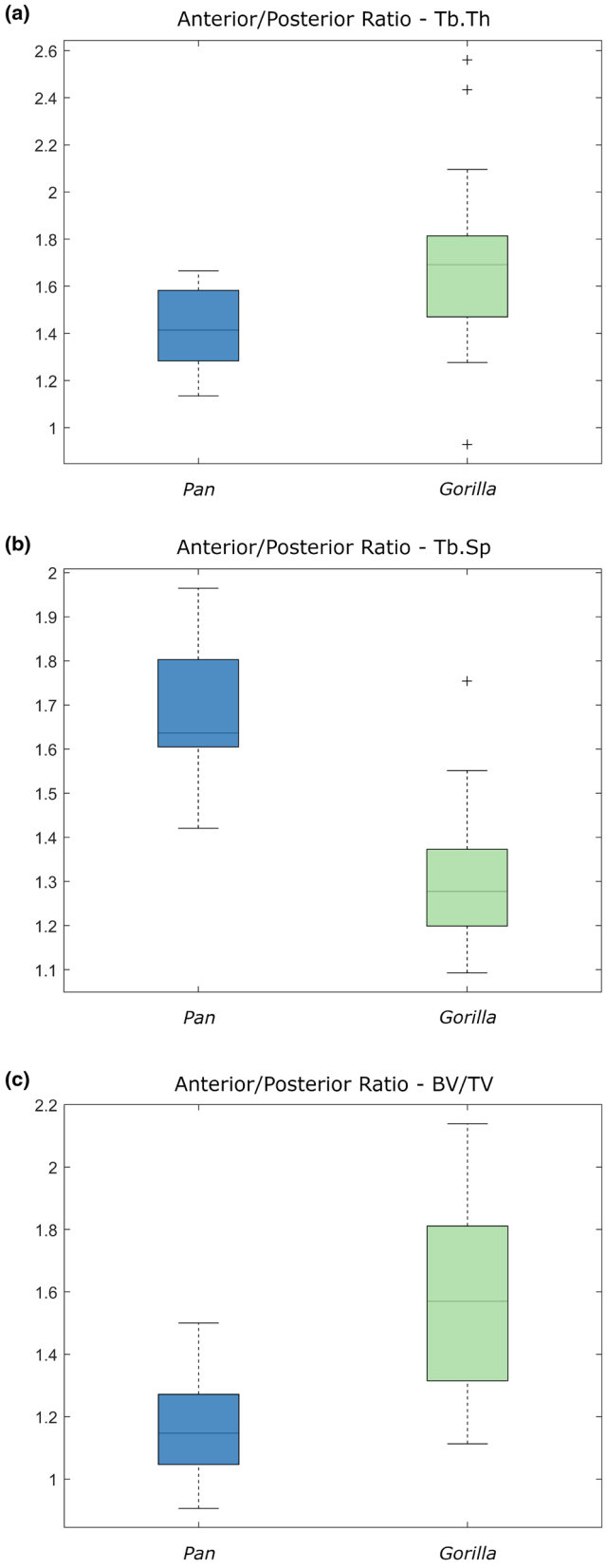

FIGURE 5 Box plots of ratios of anterior calcaneal raw parameter values/posterior calcaneal raw parameter values for (a) Tb.Th, (b) Tb.Sp, and (c) BV/TV.

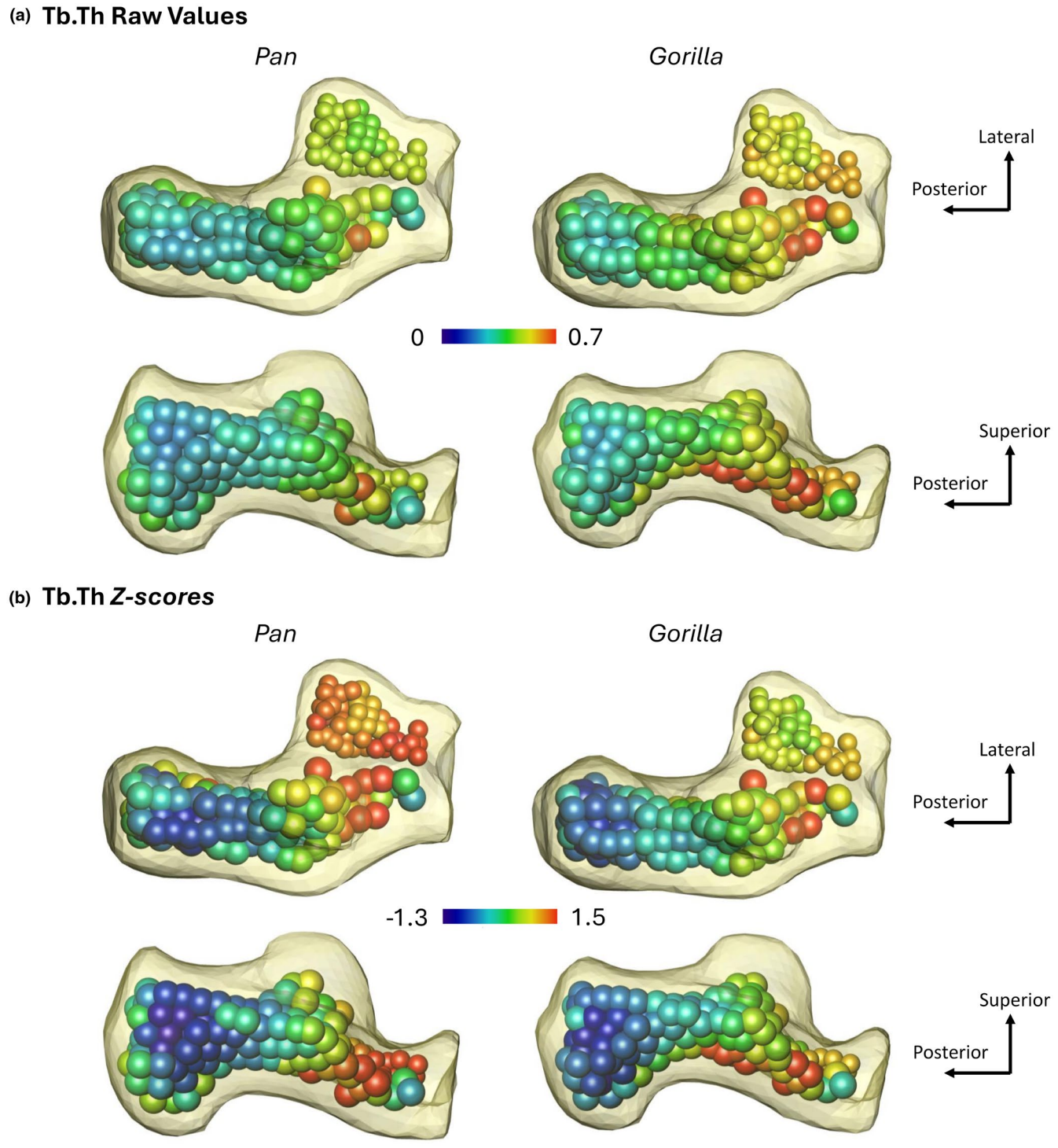

FIGURE 6 Color maps of variation in average Tb.Th (a) raw values and (b) z-scores in *Pan* and *Gorilla*. Volumes of interest are color coded based on the parameter or z-score value.

Figure S3b for a plot of PC 1 vs. 2). The *Gorilla* calcaneus is characterized by an anterior–posterior gradient in the distribution of BV/TV throughout the calcaneus, while *Pan* BV/TV is more evenly distributed with higher concentrations in the calcaneal tuberosity compared to *Gorilla* (Figure 10b).

4 | DISCUSSION

Pan and *Gorilla* significantly differ in their overall calcaneal trabecular architecture, consistent with our hypothesis. This morphological variation is likely driven by differences in degree of arboreality and

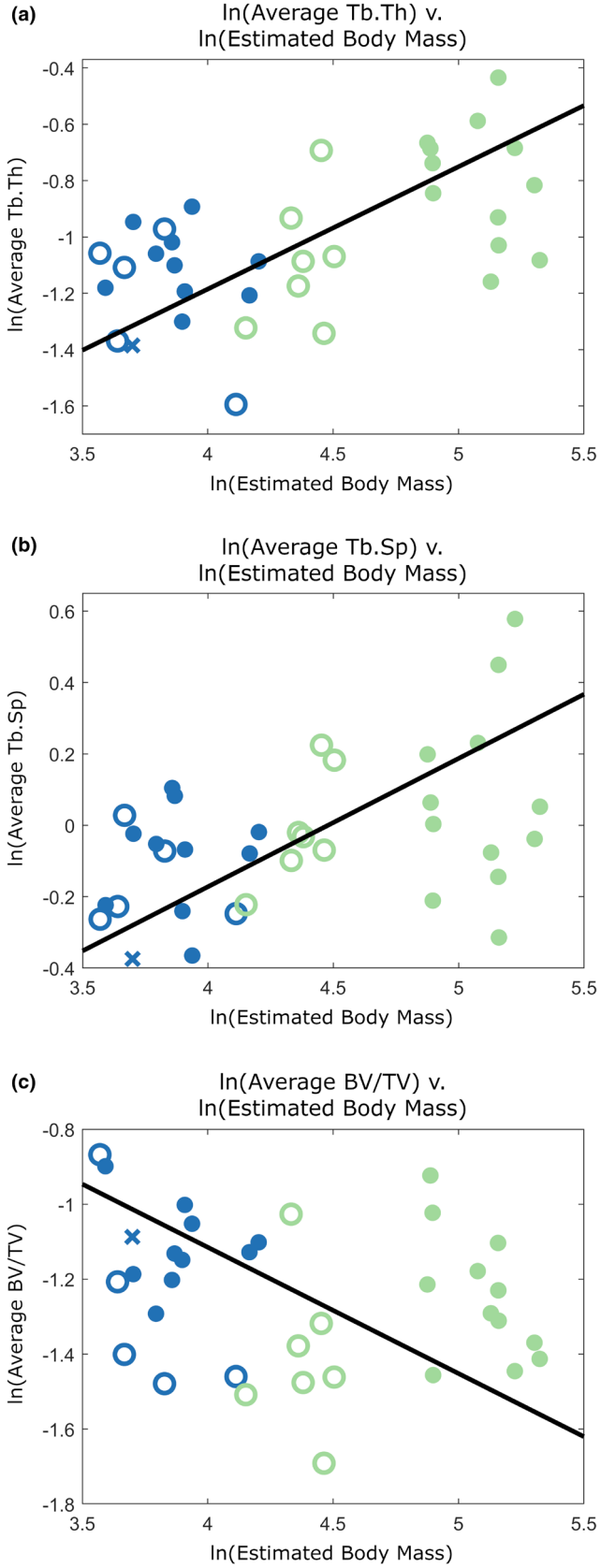

FIGURE 7 RMA regression analyses of average (a) Tb.Th, (b) Tb.Sp, and (c) BV/TV values for each specimen regressed against estimated body mass. *Gorilla* is in green, and *Pan* is in blue. Males are represented by closed circles, females open circles, and specimens of unknown sex are represented by crosses.

foot biomechanics between the taxa, rather than strictly body size differences as all measures investigated here either exhibited an isometric (Tb.Th, Tb.Sp) or non-significant (BV/TV) relationship with EBM. The lack of significant relationship between BV/TV and EBM is consistent with trends seen in the modern human calcaneus (Saers et al., 2019a, 2019b). However, this differs from previous findings of gorilla calcaneal BV/TV scaling, which demonstrated a positive allometric relationship (Harper & Patel, 2024). The difference in the scaling results between the studies is likely driven by the addition of a large number of smaller-bodied apes (i.e., *Pan* specimens) to the sample, as well as the relatively higher average BV/TV in *Pan* compared to *Gorilla*. This may reflect the inclusion of *Pan paniscus* specimens in the sample, a taxon suggested to exhibit systematically higher BV/TV (Dunmore et al., 2024). Our results also differ from findings in the humeral and femoral head of nonhuman primates (Ryan & Shaw, 2013). Given the variation in findings regarding how BV/TV varies with body size, it is important to note that the scaling analysis presented here focuses solely on the average parameter value for each specimen. It is thus possible that there is regional scaling variation or that there may be differences in calcaneal trabecular architecture related to how forces associated with body mass are transmitted through the calcaneus. More work needs to be done to understand how trabecular architecture varies both more broadly among nonhuman primates and regionally within the foot.

Both *Pan* and *Gorilla* exhibit an anteroposterior gradation of Tb.Th and BV/TV raw values with relatively higher values of both in the anterior half of the bone. The difference in trabecular parameters between the anterior and posterior calcaneus is exaggerated in *Gorilla*. This anteroposterior gradation in *Gorilla* has previously been suggested to reflect a relatively consistent pattern of load through the calcaneus (Harper & Patel, 2024). More specifically, it was proposed that the relatively thicker trabeculae in the anterior part of the bone are related to potentially higher forces associated with an anteriorly positioned center of mass (Druelle et al., 2019; Giddings et al., 2000; Harper & Patel, 2024). *Pan* exhibits a similarly positioned center of mass (Druelle et al., 2019), suggesting the less extreme anterior to posterior gradation is likely driven by either their relatively lower body mass (i.e., absolutely lower forces associated with body mass need to be transmitted through the subtalar joint) or relatively higher forces acting on the posterior calcaneus (discussed below). When z-scores are examined, however, there is a large concentration of relatively higher Tb.Th and BV/TV values in the anterior calcaneus. There is also a moderate concentration in the posterior part of the calcaneal tuberosity in *Pan*, but this is not as high as is seen in the anterior calcaneus. This suggests that the forces associated with body mass transmission are likely higher than muscle forces acting on the calcaneus, which is consistent with previous conclusions regarding the gorilla calcaneus (Harper & Patel, 2024). Empirical data on the relative forces acting on the African ape calcaneus, however, are needed to assess these hypotheses.

The relatively higher BV/TV and Tb.Th in the posterior aspect of the *Pan* calcaneal tuberosity may be indicative of potentially higher forces acting on the posterior calcaneus as a consequence of

TABLE 3 Results of RMA regressions of average trabecular parameters relative to estimated body mass.

Trabecular parameter	Slope	Intercept
Tb.Th	0.434 (0.325, 0.580)	−2.922 (−3.559, −2.445)
Tb.Sp	0.360 (0.263, 0.491)	−1.611 (−2.186, −1.189)
BV/TV	−0.337 (−0.471, 0.241)	0.233 (−0.188, 0.822)

Note: Both taxa were pooled for these analyses. 95 percent confidence intervals in parentheses.

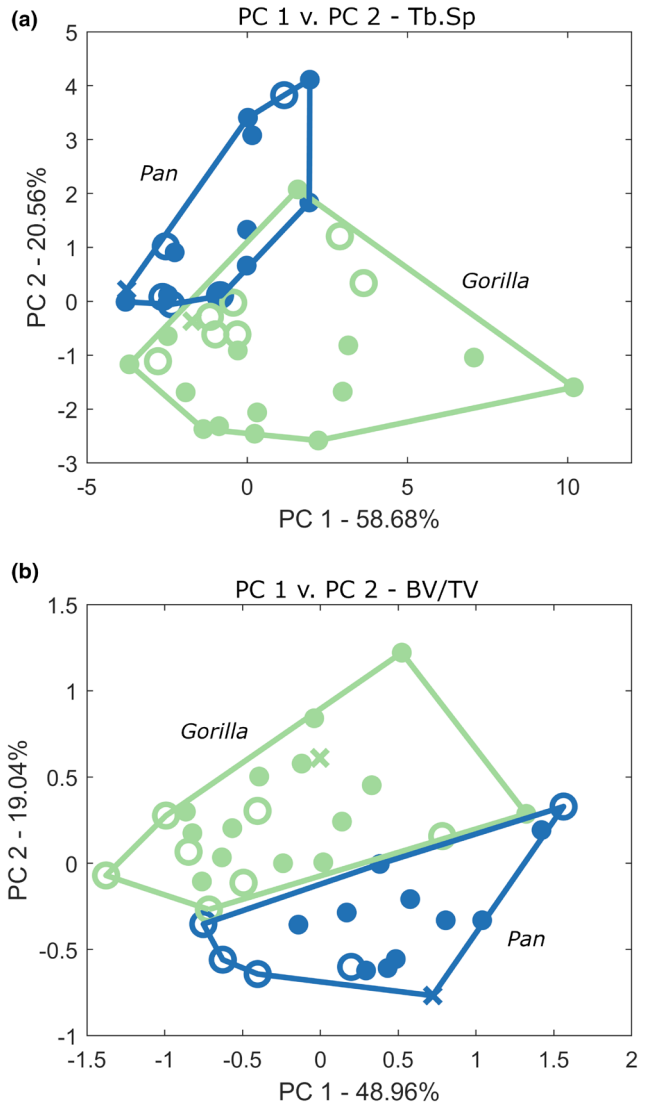

FIGURE 8 PC plots of whole-bone raw (a) Tb.Sp variation and (b) BV/TV variation. *Gorilla* is in green, and *Pan* is in blue. Males are represented by closed circles, females open circles, and specimens of unknown sex are represented by crosses.

being more arboreal. Although both African apes are arboreal, *Pan* has been observed to spend significantly more time tree climbing (Doran, 1996, 1997; Doran & Hunt, 1994; Doran & McNeilage, 1998; Doran-Sheehy et al., 2004; Ramos, 2014; Remis, 1997, 1998a, 1998b, 1999; Robbins et al., 2025; Tocheri et al., 2011). It is possible that during vertical climbing the triceps surae muscle complex (i.e., gastrocnemius and soleus) exerts a higher magnitude of force, or possibly just more sustained muscle activity in general during stance (e.g., Larson, 2025) on the bone than during terrestrial quadrupedal locomotion. Relatively higher forces on the hindlimb during climbing compared to horizontal locomotion have been observed in *Eulemur* (Hanna & Schmitt, 2011); however, we do not have such data for the African apes. This hypothesis would be consistent with the observed trend that more arboreal gorillas, specifically *G. g. gorilla* and *G. b. graueri*, exhibit relatively higher BV/TV in the posterior calcaneus than *G. b. beringei* from the Virunga mountains (Harper & Patel, 2024). It has been previously noted that during vertical climbing *Pan* has high levels of ankle dorsiflexion (DeSilva, 2009), which suggests that this would need to be counteracted by a large plantarflexor force (via the triceps surae muscle complex) to continue vertical ascent (i.e., during push-off). There is some support for this hypothesis, especially from electromyography data in the chimpanzee gastrocnemius during vertical climbing (see figure 15 in Larson, 2025). When vertical climbing was compared between *G. g. gorilla* and *P. paniscus* it was found that the two apes used different limb kinematics such that vertical climbing between the two taxa was described as being "not functionally equivalent" (Isler, 2005). Although foot and ankle kinematics of these primates have yet to be compared during vertical climbing, these findings suggest that potential kinematic differences between the genera may be driving some of the variation in calcaneal tuberosity trabecular structure. It is possible, similar to our hypothesis for *Pan*, that *Gorilla* also recruits the triceps surae muscle complex more during climbing than quadrupedal walking (as suggested by Harper & Patel, 2024); however, the effects on the trabecular structure are more pronounced in *Pan* due to the greater frequency of arboreality. Further comparisons to highly arboreal primates, such as orangutans, may help to further shed light on these questions.

Overall, the *Pan* calcaneus exhibits less trabecular spacing (based on raw parameter values) than is observed in *Gorilla*, indicating that *Pan* trabeculae are more closely packed. This is consistent with findings of a previous study looking at VOIs underlying the posterior talar facet and calcaneal tuberosity (Addison & Lieberman, 2020). The relatively lower Tb.Sp may be reflective of the proposed use of more variable foot postures in *Pan*. Due to their relatively greater arboreality, it is likely that they do not consistently load their foot in the same way due to the less predictable nature of the trees as a substrate. The higher percentage of arboreal behavior also leads to the foot utilizing more variable kinematics. Having more closely packed trabeculae may help to transmit forces coming from more variable directions. Future investigations of the degree of anisotropy may help provide more insight into calcaneal trabecular architecture and directions of foot loading. Despite the differences

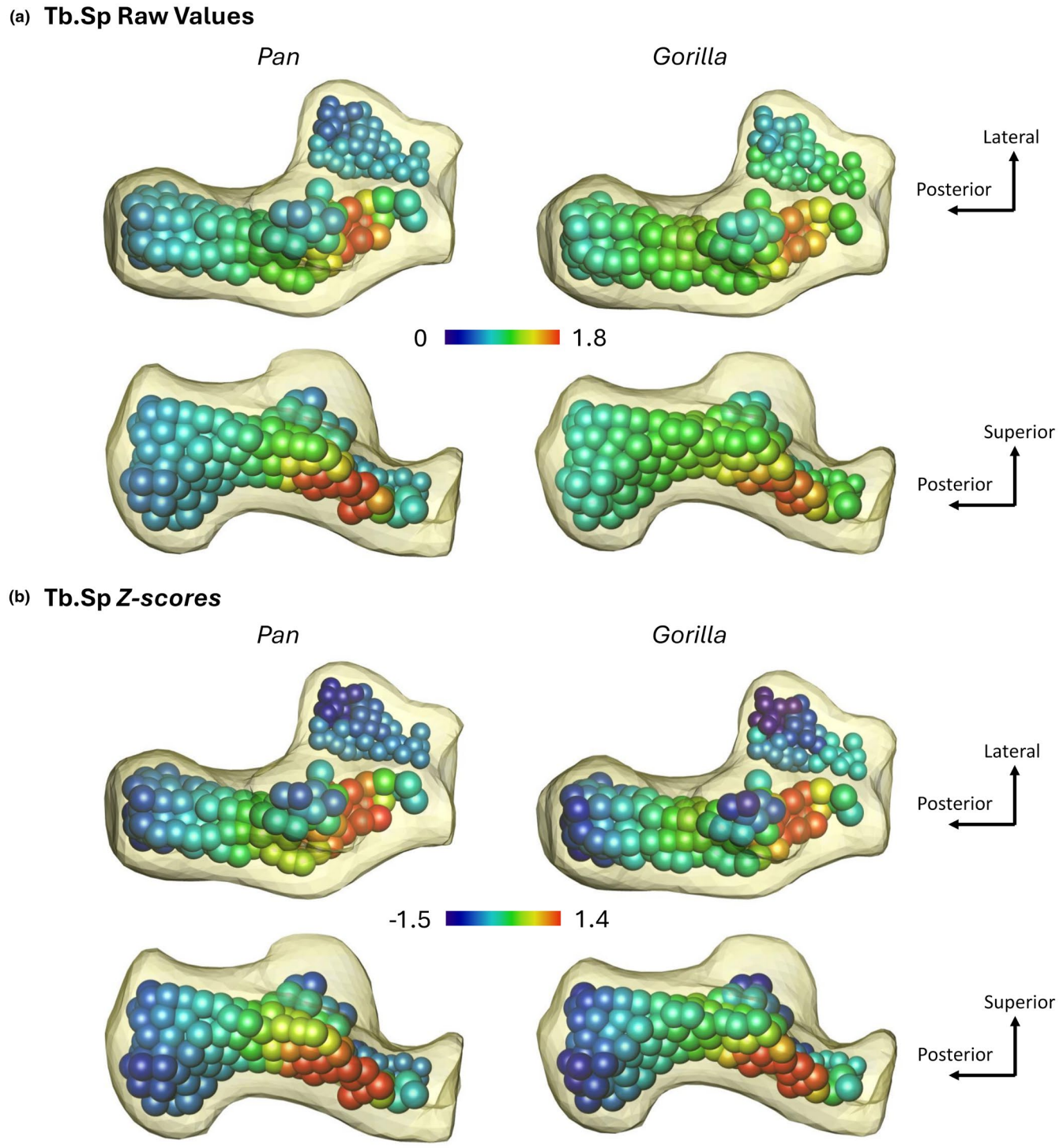

FIGURE 9 Color maps of variation in average Tb.Sp (a) raw values and (b) z-scores in *Pan* and *Gorilla*. Volumes of interest are color coded based on the parameter or z-score value.

in overall Tb.Sp, both *Pan* and *Gorilla* exhibit a relatively large region of Tb.Sp in the anterior calcaneus. This region is substantially larger in the *Pan* calcaneus than *Gorilla*; however, it does not appear to be as large as the "Ward's neutral triangle" that is observed in the human calcaneus (Bajraliu et al., 2016; see DeMars et al., 2021 for images). Direct comparisons of these taxa to humans may provide more insight into variation in this region of the bone in the hominoid calcaneus.

5 | CONCLUSIONS

Pan and *Gorilla* calcaneal trabecular architecture varies with respect to hypothesized loading differences as a consequence of differences in their use of arboreal behaviors and accompanying foot biomechanics. Both taxa exhibit an anteroposterior gradation in BV/TV and Tb.Th, although the anterior–posterior difference is exaggerated

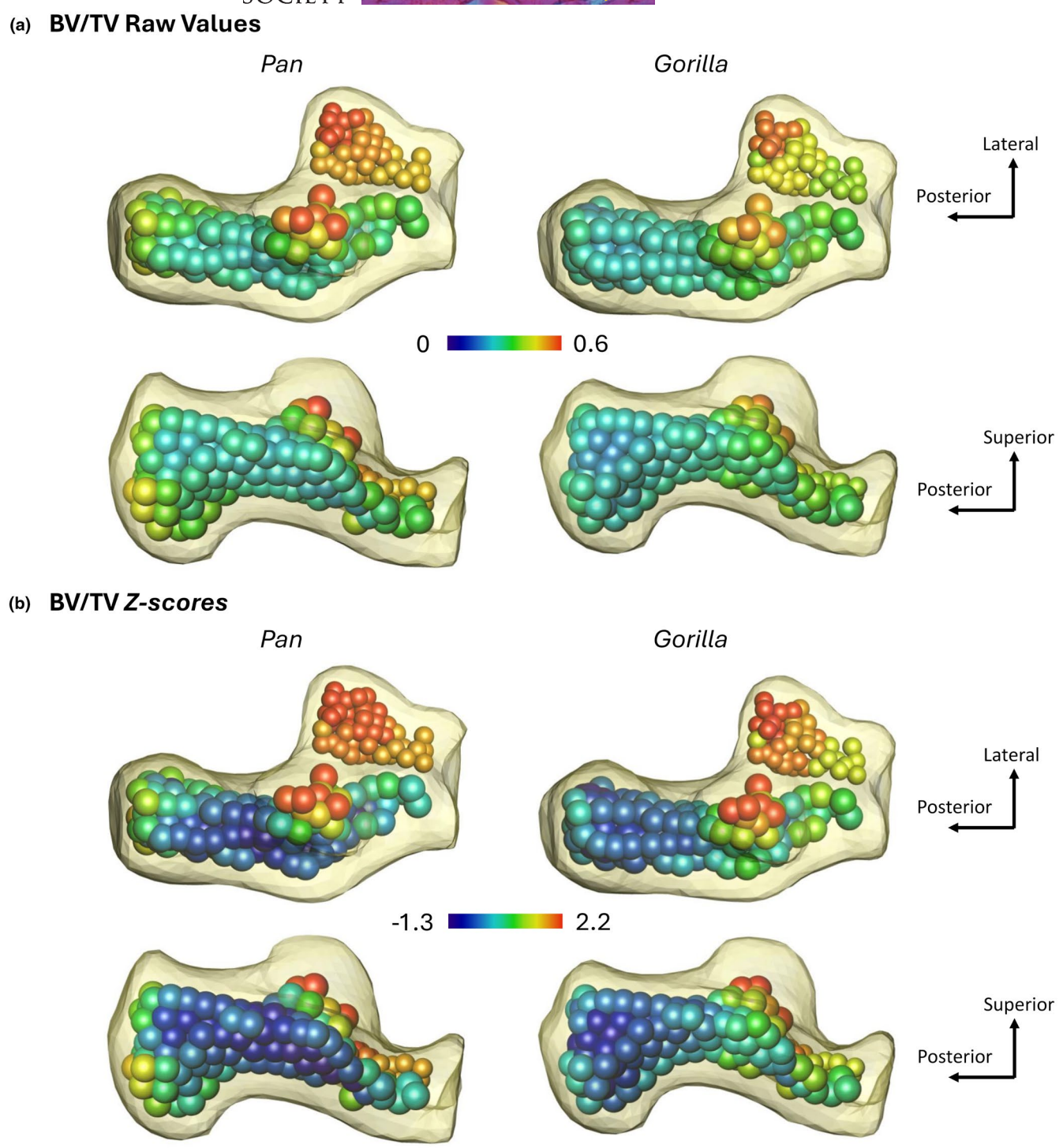

FIGURE 10 Color maps of variation in average BV/TV (a) raw values and (b) z-scores in *Pan* and *Gorilla*. Volumes of interest are color coded based on the parameter or z-score value.

in *Gorilla*, likely as an adaptation to a relatively more stereotypical foot posture. *Pan* exhibits relatively higher BV/TV and Tb.Th in the posterior aspect of the calcaneal tuberosity, which may serve as an adaptation to a relatively higher frequency of forces from the triceps surae muscle complex due to more time spent vertical climbing. These robust and consistent findings increase our understanding of how trabecular bone responds to likely forces acting on the calcaneus in plantigrade apes. Future analyses of calcaneal trabecular architecture should focus on comparisons to humans and orangutans because these taxa represent extremes in variability of foot biomechanics and degree of arboreality, allowing for further investigation of the trends observed here.

AUTHOR CONTRIBUTIONS

Christine M. Harper: Conceptualization (lead); data curation (equal); formal analysis (lead); funding acquisition (equal); investigation (lead); methodology (lead); software (lead); validation (lead); writing—original draft (lead); writing—review and editing (equal). Biren A. Patel: Data curation (equal); formal analysis (supporting); funding acquisition (equal); investigation (supporting); writing—review and editing (equal).

ACKNOWLEDGEMENTS

We would like to thank Mark Omura at the MCZ, Darrin Lunde at the USNM, and Eileen Westwig and Neil Duncan at AMNH for access to specimens in their collections. We also thank the Rwandan government for permission to study specimens curated by the Mountain Gorilla Skeletal Project, and Shannon McFarlin and Angel Zeininger for providing us with scan data. For assistance with micro-CT scanning, we thank Greg Lin and Jim Reynolds at Harvard's Center for Nanoscale Technology, and Tautis Skorka at the University of Southern California's Molecular Imaging Center.

DATA AVAILABILITY STATEMENT

Data that support the findings of this study are available from the corresponding author upon reasonable request.

ORCID

Biren A. Patel https://orcid.org/0000-0003-1844-1931

REFERENCES

Adams, D.C. & Otárola-Castillo, E. (2013) Geomorph: an r package for the collection and analysis of geometric morphometric shape data. *Methods in Ecology and Evolution*, 4, 393–399. Available from: https://doi.org/10.1111/2041-210X.12035

Addison, B.J. & Lieberman, D.E. (2020) Assessing patterns of variation in BV/TV in the calcaneus and C2 vertebra of *Gorilla gorilla*, *pan troglodytes*, and populations of Homo sapiens from the Pleistocene and Holocene that differ in physical activity levels. *American Journal of Physical Anthropology*, 173, 337–349. Available from: https://doi.org/10.1002/ajpa.24064

Athavale, S.A., Joshi, S.D. & Joshi, S.S. (2010) Internal architecture of calcaneus: correlations with mechanics and pathoanatomy of calcaneal fractures. *Surgical and Radiologic Anatomy*, 32, 115–122. Available from: https://doi.org/10.1007/s00276-009-0563-2

Bajraliu, M., Walley, K.C. & Kwon, J.Y. (2016) Rationale for the Hypodense calcaneal region of Ward's neutral triangle. *The Orthopaedic Journal at Harvard Medical School*, 17, 63–67.

Barak, M.M., Lieberman, D.E. & Hublin, J.-J. (2011) A Wolff in sheep's clothing: trabecular bone adaptation in response to changes in joint loading orientation. *Bone*, 49, 1141–1151. Available from: https://doi.org/10.1016/j.bone.2011.08.020

Bird, E.E., Kivell, T.L. & Skinner, M.M. (2022) Patterns of internal bone structure and functional adaptation in the hominoid scaphoid, lunate, and triquetrum. *American Journal of Biological Anthropology*, 177, 266–285. Available from: https://doi.org/10.1002/ajpa.24449

Boskey, A.L. & Imbert, L. (2017) Bone quality changes associated with aging and disease: a review. *Annals of the New York Academy of Sciences*, 1410, 93–106. Available from: https://doi.org/10.1111/nyas.13572

Burgess, M.L., McFarlin, S.C., Mudakikwa, A., Cranfield, M.R. & Ruff, C.B. (2018) Body mass estimation in hominoids: age and locomotor effects. *Journal of Human Evolution*, 115, 36–46. Available from: https://doi.org/10.1016/j.jhevol.2017.07.004

Canington, S.L., Sylvester, A.D., Burgess, M.L., Junno, J.-A. & Ruff, C.B. (2018) Long bone diaphyseal shape follows different ontogenetic trajectories in captive and wild gorillas. *American Journal of Physical Anthropology*, 167, 366–376. Available from: https://doi.org/10.1002/ajpa.23636

Carlson, K.J. (2005) Investigating the form-function interface in African apes: relationships between principal moments of area and positional behaviors in femoral and humeral diaphyses. *American Journal of Physical Anthropology*, 127, 312–334. Available from: https://doi.org/10.1002/ajpa.20124

Chirchir, H., Ruff, C.B., Junno, J.-A. & Potts, R. (2017) Low trabecular bone density in recent sedentary modern humans. *American Journal of Physical Anthropology*, 162, 550–560. Available from: https://doi.org/10.1002/ajpa.23138

Collyer, M.L., Sekora, D.J. & Adams, D.C. (2015) A method for analysis of phenotypic change for phenotypes described by high-dimensional data. *Heredity*, 115, 357–365. Available from: https://doi.org/10.1038/hdy.2014.75

Colombo, A., Stephens, N.B., Tsegai, Z.J., Bettuzzi, M., Morigi, M.P., Belcastro, M.G. et al. (2019) Trabecular analysis of the distal radial metaphysis during the Acquisition of Crawling and Bipedal Walking in childhood: a preliminary study. *Bulletins et Mémoires de la Société d'Anthropologie de Paris*, 31, 43–51. Available from: https://doi.org/10.3166/bmsap-2018-0041

Currey, J.D. (2013) *Bones: structure and mechanics*. Princeton, NJ: Princeton University Press.

DeMars, L.J.D., Stephens, N.B., Saers, J.P.P., Gordon, A., Stock, J.T. & Ryan, T.M. (2021) Using point clouds to investigate the relationship between trabecular bone phenotype and behavior: an example utilizing the human calcaneus. *American Journal of Human Biology*, 33, e23468. Available from: https://doi.org/10.1002/ajhb.23468

DeSilva, J., McNutt, E., Benoit, J. & Zipfel, B. (2019) One small step: a review of Plio-Pleistocene hominin foot evolution. *American Journal of Physical Anthropology*, 168, 63–140. Available from: https://doi.org/10.1002/ajpa.23750

DeSilva, J.M. (2009) Functional morphology of the ankle and the likelihood of climbing in early hominins. *Proceedings of the National Academy of Sciences*, 106, 6567–6572. Available from: https://doi.org/10.1073/pnas.0900270106

Doran, D.M. (1996) Comparative positional behavior of the African apes. In: McGrew, W.C., Marchant, L.F. & Nishida, T. (Eds.) *Great ape societies*. Cambridge: Cambridge University Press, pp. 213–224.

Doran, D.M. (1997) Ontogeny of locomotion in mountain gorillas and chimpanzees. *Journal of Human Evolution*, 32, 323–344. Available from: https://doi.org/10.1006/jhev.1996.0095

Doran, D.M. & Hunt, K.D. (1994) Comparative locomotor behavior of chimpanzees and bonobos: species and habitat differences. In: Wrangham, R.W., McGrew, W.C., de Waal, F.B. & Heltne, P.G. (Eds.) *Chimpanzee cultures*. Cambridge, MA: Harvard University Press, pp. 93–106.

Doran, D.M. & McNeilage, A. (1998) Gorilla ecology and behavior. *Evolutionary Anthropology: Issues, News, and Reviews*, 6, 120–131. Available from: https://doi.org/10.1002/(SICI)1520-6505(1998)6:4<120::AID-EVAN2>3.0.CO;2-H

Doran-Sheehy, D.M., Greer, D., Mongo, P. & Schwindt, D. (2004) Impact of ecological and social factors on ranging in western gorillas. *American Journal of Primatology*, 64(2), 207–222. Available from: https://doi.org/10.1002/ajp.20075

Doube, M., Kłosowski, M.M., Arganda-Carreras, I., Cordelières, F.P., Dougherty, R.P., Jackson, J.S. et al. (2010) BoneJ: free and extensible bone image analysis in ImageJ. *Bone*, 47, 1076–1079. Available from: https://doi.org/10.1016/j.bone.2010.08.023

Druelle, F., Berthet, M. & Quintard, B. (2019) The body center of mass in primates: is it more caudal than in other quadrupedal mammals?

American Journal of Physical Anthropology, 169, 170–178. Available from: https://doi.org/10.1002/ajpa.23813

Dunmore, C.J., Bachmann, S., Synek, A., Pahr, D.H., Skinner, M.M. & Kivell, T.L. (2024) The deep trabecular structure of first metacarpals in extant hominids. *American Journal of Biological Anthropology*, 183(3), e24695. Available from: https://doi.org/10.1002/ajpa.24695

Dunmore, C.J., Kivell, T.L., Bardo, A. & Skinner, M.M. (2019) Metacarpal trabecular bone varies with distinct hand-positions used in hominid locomotion. *Journal of Anatomy*, 235, 45–66. Available from: https://doi.org/10.1111/joa.12966

Eriksen, E.F. & Glerup, H. (2000) Pathogenesis of osteoporosis. In: Obrant, K. (Ed.) *Management of Fractures in severely osteoporotic bone*. London: Springer, pp. 13–32.

Eriksen, E.F., Mosekilde, L. & Melsen, F. (1985) Trabecular bone remodeling and bone balance in hyperthyroidism. *Bone*, 6, 421–428. Available from: https://doi.org/10.1016/8756-3282(85)90218-2

Fajardo, R.J., Müller, R., Ketcham, R.A. & Colbert, M. (2007) Nonhuman anthropoid primate femoral neck trabecular architecture and its relationship to locomotor mode. *The Anatomical Record*, 290, 422–436. Available from: https://doi.org/10.1002/ar.20493

FEI Visualization Sciences Group. (2015) *Avizo Lite 9.0.1*. Hillsboro: FEI Company.

Figus, C., Carlson, K.J., Bortolini, E., Saers, J., Seghi, F., Sorrentino, R. et al. (2025) The ontogeny of the human calcaneus: insights from morphological and trabecular changes during postnatal growth. *American Journal of Biological Anthropology*, 186, e70007. Available from: https://doi.org/10.1002/ajpa.70007

Figus, C., Stephens, N.B., Sorrentino, R., Bortolini, E., Arrighi, S., Higgins, O.A. et al. (2023) Morphologies in-between: the impact of the first steps on the human talus. *The Anatomical Record*, 306, 124–142. Available from: https://doi.org/10.1002/ar.25010

Figus, C., Stephens, N.B., Sorrentino, R., Bortolini, E., Arrighi, S., Lugli, F. et al. (2022) Human talar ontogeny: insights from morphological and trabecular changes during postnatal growth. *American Journal of Biological Anthropology*, 179, 211–228. Available from: https://doi.org/10.1002/ajpa.24596

Gebo, D.L. (1992) Plantigrady and foot adaptation in African apes: implications for hominid origins. *American Journal of Physical Anthropology*, 89, 29–58. Available from: https://doi.org/10.1002/ajpa.1330890105

Gefen, A. & Seliktar, R. (2004) Comparison of the trabecular architecture and the isostatic stress flow in the human calcaneus. *Medical Engineering & Physics*, 26, 119–129. Available from: https://doi.org/10.1016/j.medengphy.2003.10.003

Giddings, V.L., Beaupré, G.S., Whalen, R.T. & Carter, D.R. (2000) Calcaneal loading during walking and running. *Medicine & Science in Sports & Exercise*, 32(3), 627–634.

Gierse, H. (1976) The cancellous structure in the calcaneus and its relation to mechanical stressing. *Anatomy and Embryology*, 150, 63–83. Available from: https://doi.org/10.1007/BF00346287

Glatt, V., Canalis, E., Stadmeyer, L. & Bouxsein, M.L. (2007) Age-related changes in trabecular architecture differ in female and male C57BL/6J mice. *Journal of Bone and Mineral Research*, 22, 1197–1207. Available from: https://doi.org/10.1359/jbmr.070507

Gower, J.C. (1975) Generalized procrustes analysis. *Psychometrika*, 40, 33–51. Available from: https://doi.org/10.1007/BF02291478

Gross, T., Kivell, T.L., Skinner, M.M., Nguyen, H. & Pahr, D.H. (2014) Holistic analysis of bone. *Palaeontologia Electronica*, 17, 1.

Gunz, P., Mitteroecker, P. & Bookstein, F.L. (2005) Semilandmarks in three dimensions. In: Slice, D.E. (Ed.) *Modern morphometrics in physical anthropology*. New York: Springer, pp. 73–98.

Hanna, J.B. & Schmitt, D. (2011) Interpreting the role of climbing in primate locomotor evolution: are the biomechanics of climbing influenced by habitual substrate use and anatomy? *International Journal of Primatology*, 32(2), 430–444. Available from: https://doi.org/10.1007/s10764-010-9479-2

Harper, C.M. (2023) Human calcaneal variation relative to subsistence strategy, activity level, and footwear. *Frontiers in Earth Science*, 11, 1213374. Available from: https://doi.org/10.3389/feart.2023.1213374

Harper, C.M. & Patel, B.A. (2024) Trabecular bone variation in the gorilla calcaneus. *American Journal of Biological Anthropology*, 184, e24939. Available from: https://doi.org/10.1002/ajpa.24939

Harper, C.M., Ruff, C.B. & Sylvester, A.D. (2021) Gorilla calcaneal morphological variation and ecological divergence. *American Journal of Physical Anthropology*, 174, 49–65. Available from: https://doi.org/10.1002/ajpa.24135

Huiskes, R., Ruimerman, R., Van Lenthe, G.H. & Janssen, J.D. (2000) Effects of mechanical forces on maintenance and adaptation of form in trabecular bone. *Nature*, 405, 704–706. Available from: https://doi.org/10.1038/35015116

Isler, K. (2005) 3D-kinematics of vertical climbing in hominoids. *American Journal of Physical Anthropology*, 126, 66–81. Available from: https://doi.org/10.1002/ajpa.10419

Jacobs, C.R. (2000) The mechanobiology of cancellous bone structural adaptation. *Journal of Rehabilitation Research and Development*, 37, 209–216.

Jungers, W.L. & Susman, R.L. (1984) Body size and skeletal allometry in African apes. In: Susman, R.L. (Ed.) *The pygmy chimpanzee: evolutionary biology and behavior*. Boston, MA: Springer, pp. 131–177.

Kidd, R. (1999) Evolution of the rearfoot. A model of adaptation with evidence from the fossil record. *Journal of the American Podiatric Medical Association*, 89, 2–17. Available from: https://doi.org/10.7547/87507315-89-1-2

Kirchhoff, C., Braunstein, V., Milz, S., Sprecher, C.M., Kirchhoff, S., Graw, M. et al. (2012) Age and gender as determinants of the bone quality of the greater tuberosity: a HR-pQCT cadaver study. *BMC Musculoskeletal Disorders*, 13, 221. Available from: https://doi.org/10.1186/1471-2474-13-221

Kivell, T.L. (2016) A review of trabecular bone functional adaptation: what have we learned from trabecular analyses in extant hominoids and what can we apply to fossils? *Journal of Anatomy*, 228, 569–594. Available from: https://doi.org/10.1111/joa.12446

Kivell, T.L., Skinner, M.M., Lazenby, R. & Hublin, J.-J. (2011) Methodological considerations for analyzing trabecular architecture: an example from the primate hand. *Journal of Anatomy*, 218, 209–225. Available from: https://doi.org/10.1111/j.1469-7580.2010.01314.x

Koneru, M.C. & Harper, C.M. (2024) Comparing lateral plantar process trabecular structure to other regions of the human calcaneus. *The Anatomical Record*, 307, 3152–3165. Available from: https://doi.org/10.1002/ar.25406

Lanham-New, S.A. (2008) Importance of calcium, vitamin D and vitamin K for osteoporosis prevention and treatment: symposium on 'diet and bone health'. *Proceedings of the Nutrition Society*, 67, 163–176. Available from: https://doi.org/10.1017/S0029665108007003

Larson, S.G. (2025) Chimpanzee hind limb muscle electromyographic activity patterns during locomotion. *Journal of Human Evolution*, 208, 103751. Available from: https://doi.org/10.1016/j.jhevol.2025.103751

Lazenby, R.A., Skinner, M.M., Hublin, J.-J. & Boesch, C. (2011) Metacarpal trabecular architecture variation in the chimpanzee (*pan troglodytes*): evidence for locomotion and tool-use? *American Journal of Physical Anthropology*, 144, 215–225. Available from: https://doi.org/10.1002/ajpa.21390

Lloyd, S. (1982) Least squares quantization in PCM. *IEEE Transactions on Information Theory*, 28, 129–137. Available from: https://doi.org/10.1109/TIT.1982.1056489

Lukova, A., Bachmann, S., Synek, A., Pahr, D.H., Kilbourne, B., Dunmore, C.J. et al. (2025) Trabecular architecture of the proximal tibia in

extant hominids. *American Journal of Biological Anthropology*, 187, e70084. Available from: https://doi.org/10.1002/ajpa.70084

Maga, M., Kappelman, J., Ryan, T.M. & Ketcham, R.A. (2006) Preliminary observations on the calcaneal trabecular microarchitecture of extant large-bodied hominoids. *American Journal of Physical Anthropology*, 129, 410–417. Available from: https://doi.org/10.1002/ajpa.20276

Majumdar, S., Genant, H.K., Grampp, S., Newitt, D.C., Truong, V.-H., Lin, J.C. et al. (1997) Correlation of trabecular bone structure with age, bone mineral density, and osteoporotic status: in vivo studies in the distal radius using high resolution magnetic resonance imaging. *Journal of Bone and Mineral Research*, 12, 111–118. Available from: https://doi.org/10.1359/jbmr.1997.12.1.111

Marchi, D., Harper, C.M., Chirchir, H. & Ruff, C.B. (2019) Relative fibular strength and locomotor behavior in KNM-WT 15000 and OH 35. *Journal of Human Evolution*, 131, 48–60. Available from: https://doi.org/10.1016/j.jhevol.2019.02.005

McNutt, E.J., Zipfel, B. & DeSilva, J.M. (2018) The evolution of the human foot. *Evolutionary Anthropology: Issues, News, and Reviews*, 27, 197–217. Available from: https://doi.org/10.1002/evan.21713

Nozaki, S., Amano, H., Oishi, M. & Ogihara, N. (2021) Morphological differences in the calcaneus among extant great apes investigated by three-dimensional geometric morphometrics. *Scientific Reports*, 11, 20889. Available from: https://doi.org/10.1038/s41598-021-99942-1

Orr, C.M. (2005) Knuckle-walking anteater: a convergence test of adaptation for purported knuckle-walking features of African Hominidae. *American Journal of Physical Anthropology*, 128(3), 639–658. Available from: https://doi.org/10.1002/ajpa.20192

Patel, B.A. (2024) Medial metatarsal rigidity in extant non-human catarrhine primates. *American Journal of Biological Anthropology*, 183, e24706. Available from: https://doi.org/10.1002/ajpa.24706

Pearson, O.M. & Lieberman, D.E. (2004) The aging of Wolff's 'law': ontogeny and responses to mechanical loading in cortical bone. *American Journal of Physical Anthropology*, 125, 63–99. Available from: https://doi.org/10.1002/ajpa.20155

Prang, T.C. (2015) Calcaneal robusticity in Plio-Pleistocene hominins: implications for locomotor diversity and phylogeny. *Journal of Human Evolution*, 80, 135–146. Available from: https://doi.org/10.1016/j.jhevol.2014.09.001

Prang, T.C. (2016) The subtalar joint complex of *Australopithecus sediba*. *Journal of Human Evolution*, 90, 105–119. Available from: https://doi.org/10.1016/j.jhevol.2015.10.009

R Core Team. (2021) R: a language for environment for statistical computing. R Foundation for Statistical Computing. Available from: https://R-project.org

Ramos, G.L. (2014) *Positional behavior of pan paniscus at Lui Kotale, Democratic Republic of Congo*. (Doctoral Dissertation). Indiana University.

Remis, M.J. (1997) Western lowland gorillas (*Gorilla gorilla gorilla*) as seasonal frugivores: use of variable resources. *American Journal of Primatology*, 43, 87–109. Available from: https://doi.org/10.1002/(SICI)1098-2345(1997)43:2<87::AID-AJP1>3.0.CO;2-T

Remis, M.J. (1998a) *Feeding ecology and positional behavior of Western lowland gorilla (Gorilla gorilla gorilla) in the Central African Republic* (Doctoral Dissertation). Yale University.

Remis, M.J. (1998b) The gorilla paradox: the effects of body size and habitat on positional behavior of lowland and mountain gorillas. In: Strasser, E., Fleagle, J., Rosenberger, A.L. & McHenry, H. (Eds.) *Primate locomotion*. Boston, MA: Springer, pp. 95–106.

Remis, M.J. (1999) Tree structure and sex differences in arboreality among western lowland gorillas (Gorilla gorilla gorilla) at Bai Hokou, Central African Republic. *Primates*, 40, 383–396. Available from: https://doi.org/10.1007/BF02557560

Reznikov, N., Liang, H., McKee, M.D. & Piché, N. (2022) Technical note: mapping of trabecular bone anisotropy and volume fraction in 3D using μCT images of the human calcaneus. *American Journal of Biological Anthropology*, 177, 566–580. Available from: https://doi.org/10.1002/ajpa.24474

Robbins, M.M., Drummond-Clarke, R.C., Robbins, A.M., Ostrofsky, K.R. & Kivell, T.L. (2025) Gorillas are arboreal apes. *Current Biology*, 35, 2974–2979.e3. Available from: https://doi.org/10.1016/j.cub.2025.05.015

Rohlf, F.J. & Slice, D. (1990) Extensions of the Procrustes method for the optimal superimposition of landmarks. *Systematic Zoology*, 39, 40–59. Available from: https://doi.org/10.2307/2992207

Ruff, C., Holt, B. & Trinkaus, E. (2006) Who's afraid of the big bad Wolff?: 'Wolff's law' and bone functional adaptation. *American Journal of Physical Anthropology*, 129, 484–498. Available from: https://doi.org/10.1002/ajpa.20371

Ruff, C.B., Burgess, M.L., Squyres, N., Junno, J.-A. & Trinkaus, E. (2018) Lower limb articular scaling and body mass estimation in Pliocene and Pleistocene hominins. *Journal of Human Evolution*, 115, 85–111. Available from: https://doi.org/10.1016/j.jhevol.2017.10.014

Ruff, C.B. & Runestad, J.A. (1992) Primate limb bone structural adaptations. *Annual Review of Anthropology*, 21, 407–433. Available from: https://doi.org/10.1146/annurev.an.21.100192.002203

Ryan, T.M. & Shaw, C.N. (2012) Unique suites of trabecular bone features characterize locomotor behavior in human and non-human anthropoid primates. *PLoS One*, 7, e41037. Available from: https://doi.org/10.1371/journal.pone.0041037

Ryan, T.M. & Shaw, C.N. (2013) Trabecular bone microstructure scales allometrically in the primate humerus and femur. *Proceedings of the Royal Society of London B: Biological Sciences*, 280, 20130172. Available from: https://doi.org/10.1098/rspb.2013.0172

Saers, J.P.P., DeMars, L.J., Stephens, N.B., Jashashvili, T., Carlson, K.J., Gordon, A.D. et al. (2021) Combinations of trabecular and cortical bone properties distinguish various loading modalities between athletes and controls. *American Journal of Physical Anthropology*, 174, 434–450. Available from: https://doi.org/10.1002/ajpa.24176

Saers, J.P.P., Gordon, A.D., Ryan, T.M. & Stock, J.T. (2022) Growth and development of trabecular structure in the calcaneus of Japanese macaques (Macaca fuscata) reflects locomotor behavior, life history, and neuromuscular development. *Journal of Anatomy*, 241, 67–81. Available from: https://doi.org/10.1111/joa.13641

Saers, J.P.P., Ryan, T.M. & Stock, J.T. (2019a) Trabecular bone functional adaptation and sexual dimorphism in the human foot. *American Journal of Physical Anthropology*, 168, 154–169. Available from: https://doi.org/10.1002/ajpa.23732

Saers, J.P.P., Ryan, T.M. & Stock, J.T. (2019b) Trabecular bone structure scales allometrically in the foot of four human groups. *Journal of Human Evolution*, 135, 102654. Available from: https://doi.org/10.1016/j.jhevol.2019.102654

Sarringhaus, L.A., Stock, J.T., Marchant, L.F. & McGrew, W.C. (2005) Bilateral asymmetry in the limb bones of the chimpanzee (*pan troglodytes*). *American Journal of Physical Anthropology*, 128, 840–845. Available from: https://doi.org/10.1002/ajpa.20190

Schneider, C.A., Rasband, W.S. & Eliceiri, K.W. (2012) NIH image to ImageJ: 25 years of image analysis. *Nature Methods*, 9, 671–675.

Smith, R.J. & Jungers, W.L. (1997) Body mass in comparative primatology. *Journal of Human Evolution*, 32, 523–559. Available from: https://doi.org/10.1006/jhev.1996.0122

Sokal, R.R. & Rohlf, F.J. (1998) *Biometry: the principles and practice of statistics in biological research*, third edition. New York, NY: W.H. Freeman and Company.

Sorrentino, R., Carlson, K.J., Figus, C., Pietrobelli, A., Stephens, N.B., DeMars, L.J.D. et al. (2022) The talar morphology of a hypochondroplasic dwarf: a case study from the Italian late antique period. *International Journal of Osteoarchaeology*, 32, 429–443. Available from: https://doi.org/10.1002/oa.3078

Sorrentino, R., Stephens, N.B., Marchi, D., DeMars, L.J.D., Figus, C., Bortolini, E. et al. (2021) Unique foot posture in Neanderthals

reflects their body mass and high mechanical stress. *Journal of Human Evolution*, 161, 103093. Available from: https://doi.org/10.1016/j.jhevol.2021.103093

Swartz, S.M. & Biewener, A.A. (1992) Shape and scaling. In: Biewener, A.A. (Ed.) *Biomechanics—structures and systems: a practical approach*. Oxford: Oxford University Press, pp. 21–30.

Syeda, S.M., Tsegai, Z.J., Cazenave, M., Skinner, M.M. & Kivell, T.L. (2024) Cortical bone architecture of hominid intermediate phalanges reveals functional signals of locomotion and manipulation. *American Journal of Biological Anthropology*, 184, e24902. Available from: https://doi.org/10.1002/ajpa.24902

Sylvester, A.D. & Terhune, C.E. (2017) Trabecular mapping: leveraging geometric morphometrics for analyses of trabecular structure. *American Journal of Physical Anthropology*, 163, 553–569. Available from: https://doi.org/10.1002/ajpa.23231

Tocheri, M.W., Solhan, C.R., Orr, C.M., Femiani, J., Frohlich, B., Groves, C.P. et al. (2011) Ecological divergence and medial cuneiform morphology in gorillas. *Journal of Human Evolution*, 60, 171–184. Available from: https://doi.org/10.1016/j.jhevol.2010.09.002

Warton, D.I., Duursma, R.A., Falster, D.S. & Taskinen, S. (2012) Smatr 3– an R package for estimation and inference about allometric lines. *Methods in Ecology and Evolution*, 3, 257–259. Available from: https://doi.org/10.1111/j.2041-210X.2011.00153.x

Wolff, J. (1892) *The law of bone transformation*. Berlin, Germany: Hirschwald.

Zeininger, A., Patel, B.A., Zipfel, B. & Carlson, K.J. (2016) Trabecular architecture in the StW 352 fossil hominin calcaneus. *Journal of Human Evolution*, 97, 145–158. Available from: https://doi.org/10.1016/j.jhevol.2016.05.009

Zioupos, P. & Currey, J.D. (1998) Changes in the stiffness, strength, and toughness of human cortical bone with age. *Bone*, 22, 57–66. Available from: https://doi.org/10.1016/S8756-3282(97)00228-7

SUPPORTING INFORMATION

Additional supporting information can be found online in the Supporting Information section at the end of this article.

How to cite this article: Harper, C.M. & Patel, B.A. (2026) Functional morphology of trabecular bone in the calcaneus of African apes. *Journal of Anatomy*, 00, 1–16. Available from: https://doi.org/10.1111/joa.70141